Int. J. Electrochem. Sci., 12 **(2017)** 230 – 239, doi: 10.20964/2017.01.13

International Journal of
ELECTROCHEMICAL
SCIENCE
www.electrochemsci.org

Evaluations of Fuel and Air Flow Distributing Qualities within SOFC Stack Designs with Flow Manifolds Penetrated Through Cell Plane

Shichuan Su[1], Shundong Zhang[1], Cheng Yan[1], Zongming Yang[1,], Fa Zheng[2], Li Zhang[2]*

[1] School of Energy and Power Engineering, Jiangsu University of Science and Technology, Zhenjiang, Jiangsu 212003, China.
[2] Jiangsu Zhongjing New Energy Science & Technology Research Center, Zhenjiang, Jiangsu 212013, China.
[*]E-mail: zmyang02@163.com

Received: 3 October 2016 / *Accepted:* 18 November 2016 / *Published:* 12 December 2016

In order to achieve simply manufacturing process and higher volumetric power density, many planar SOFC stacks were designed to place fuel and air manifolds within the cell unit area and penetrated it. The fuel and air flow distribution qualities within these type SOFC stacks was analyzed by 3D calculating fluid dynamics (CFD) simulating, and the following results could be concluded: i) while the fuel manifolds were placed within the SOFC unit area and penetrated through it, over 31% air flow would pass through the semicircle zones of the fuel manifold zones; iii) over 14% of the fuel flow would pass through the semicircle zone of the air manifold zone; iv) while the flow manifolds were penetrated through the cell unit plane, both the fuel and air flow distribution qualities over each cell unit would not be greatly improved by adding additional distributors or enlarging the overall outlet manifold areas.

Keywords: planar SOFC stack, flow path optimization, manifolds penetrated through SOFC unit area, 3D calculated fluid dynamics.

1. INTRODUCTION

Planar solid oxide fuel cell (SOFC) is considered to be one of the promising power conversion devices due to many favorable properties, such as fuel flexibility, compactness, high volumetric and gravimetric power densities [1-9]. However, the further development of SOFCs faces the challenges to minimize the unwanted temperature variation throughout the whole stack, which contributes to the thermal stress between different components [10-14]. Overloading of the local areas within a SOFC

cell unit or in stack component will result in failure and subsequent progressive degradation of the SOFC stack as a whole. Thus, even loading and keeping current induced degradation processes constantly distributed throughout the stack are essential to extend the overall stack lifetime [15-18]. These will rely on the proper air flow path design to ensure high air flow distribution qualities within the stack.

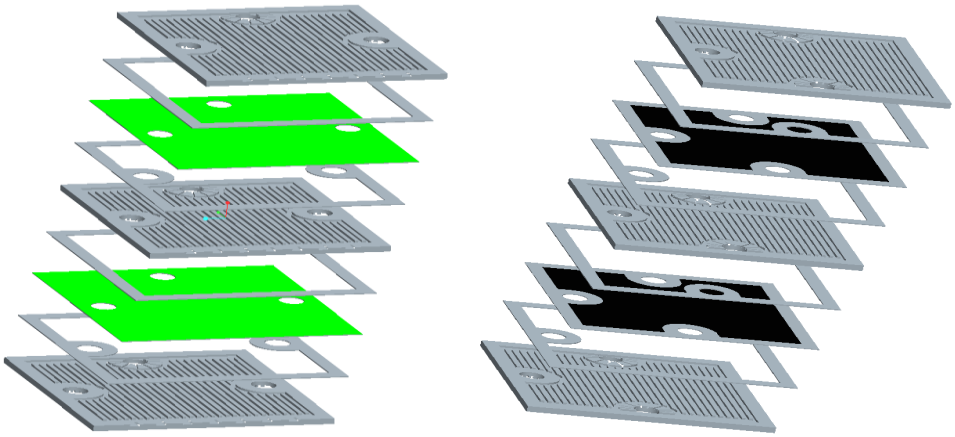

Figure 1. Sketch diagram of a planar SOFC stack design with fuel and air manifolds placed within the SOFC cell areas and penetrated through it.

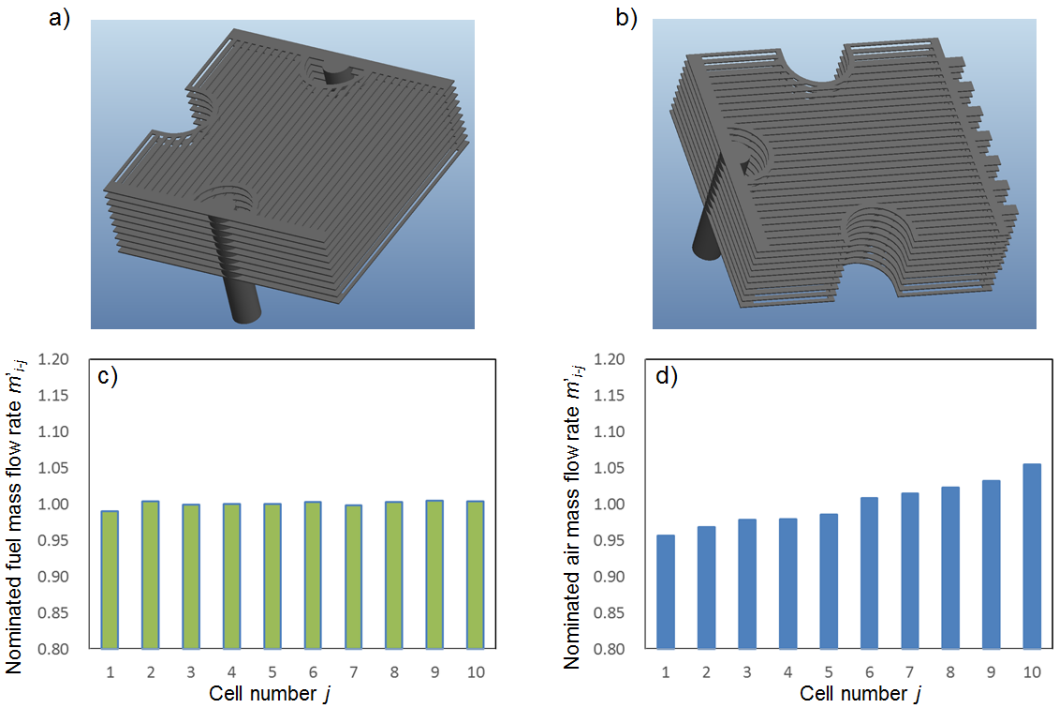

Figure 2. a) 3D fuel flow path model within 10-cell planer SOFC stack in Fig. 1; b) the corresponding 3D air flow path model; c) the nominated fuel flow rates fed to each cell layer as a function of the cell number j; d) the nominated air flow rates distribution among the piled cell layers.

In the past decade, great attentions were paid to investigate the proper structure designs for fuel

and air flow paths to achieve high stack performance and lifetime [19-27]. In order to achieve simply manufacturing process and high volumetric power density of SOFC stacks, both the fuel and air manifolds were always designed to be placed within the fuel cell unit zone and penetrated through it [28-31]. According to the designs reported by W. Wang et al. [28, 31], a typical planar SOFC stack structure with this characteristic is displayed in Fig. 1. Obviously, the fuel and air flow direction relationship can be called as cross flow management. One fuel flow inlet manifold and one outlet manifold are placed face to face at the opposite sides of the interconnector. Their effects were feeding the fuel flows to each SOFC unit and collecting exhaust gas. The radii of manifolds are 5 mm. Both them penetrate through the fuel cell plane. There are 20 rib channels (1 mm*1 mm*10 cm for each rib channel) with interval 1 mm within each solid oxide fuel cell unit. Similarly, there is one air flow inlet manifold is penetrated through the fuel cell plane, and the exhaust air flows are directly expelled to the environment.

In this paper, the fuel and air distribution characteristics within these typical planar SOFC stacks with flow manifolds penetrated through fuel cell plane were assessed by the 3D CFD model developing and simulating. Then, the fuel and flow distributions qualities within different flow path structure improving tries, such as, with circle configuration, flow distributors and different inlet and outlet manifold areas ratios were investigated to carefully analyzed to evaluate the practicable of the current manifold position designs.

2. THEORY AND METHOD

Fig. 2a and b shows the relevant fuel and air flow path models, which adopts the U-type manifolds configuration, within the 10-cell modular stacks. The active area of each SOFC unit within the stack S is around 10 cm $\times$10 cm. For the case with average output current density j around 7000 A m^{-2} and the effective utilizations of fuel and air flows η are around 80% and 20% , respectively, the fuel and air mass flow velocities at the inlet manifold entrances can be respectively calculated as [32],

$$u_{\text{fuel}} = \frac{1}{\rho_{\text{fuel}} A_{\text{in}}} \frac{NjSM_{\text{fuel}}}{4F\eta_{\text{fuel}}\chi_{\text{H}_2}} = 6.03\ \text{m s}^{-1}$$
$$u_{\text{air}} = \frac{1}{\rho_{\text{air}} A_{\text{in}}} \frac{NjSM_{\text{air}}}{4F\eta_{\text{air}}\chi_{\text{O}_2}} = 32.33\ \text{m s}^{-1} \qquad (1)$$

where F is the total electric column of one molar electrons. M_{fuel} and M_{air} are the molar mass of fuel and air, respectively. χ_{H_2} and χ_{O_2} are the mass fractions of hydrogen and oxygen within fuel and air mixtures, respectively. ρ is the mass density of mixture gas. $A_{\text{in}} = \pi r_{\text{in}}^2$ is the total areas of inlet manifold entrances. Herein, r_{in} is around 5 mm.

Finally, the fluid flow characteristics within these planar SOFC stack with manifolds penetrating through the cell unit zone would be figured out by the 3D CFD approach using software Fluent with a tolerance 1×10^{-5}. The detailed process of 3D model developing, meshing and simulating processes could be found in many previous papers [33-36]. Enough hexagonal mesh elements (i.e., 276000 for air flow path and 222000 for fuel flow path) are addred to the current 3D CFD flow path models to ensure the accuracy. For fuel flow field, the laminar flow model is addressed. As the flow

distribution within air flow path is found to be of typical turbulent flow characteristic, the k-ε calculating model is addressed.

3. RESULTS AND DISCUSSION

Fig. 2c and d show the nominated fuel and air flow rates fed to each cell layer as a function of the cell numbers, respectively. Obviously, for these 10-cells small scale planar SOFC stacks using U-type, there are relevant high fuel and air flow fed rates distributions among the piled cell layer on stack level. Thus, the attentions should be further focused on the fuel and air distributing qualities among the rib channels on single cell level. They will greatly represent the distribution quality of electrochemical performance over each SOFC unit surface [37]. As reported by Z. Yu, G. Jung and J. Myung et al. [38, 39], this will affect the stack overall performance and its working lifetime.

Fig. 3a and b illustrate the configurations of fuel and air flow distributing paths over the SOFC unit surface, respectively. Both the fuel and air flow manifolds are placed within the SOFC unit area and penetrate through it. As shown in Fig. 3a, beside the fuel flow fed header, there is a semicircle. Both them act as a fuel flow distributor. On the opposite side, there are also fed header and semicircle paths that act as an exhaust fuel gas collector. For Fig. 3b, similar flow fed header and semicircle are adopted to distribute the air flow to the rib channels. On the opposite side, exhaust air flows are directly expelled to the environment.

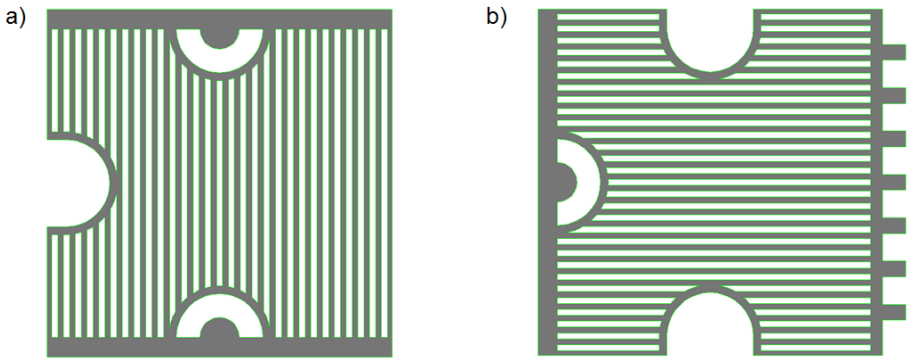

Figure 3. Sketch diagram of a planar SOFC stack design with semicircle distributors, while places the flow manifolds within the cell unit plane: a) configuration of fuel flow distribution path; b) configuration of air flow distribution path.

Fig. 4a shows the fuel flow velocity distribution among the rib channels. Obviously, most of the fuel flows are concentrated around the three semicircle zones (i.e., two semicircles for fuel flow manifolds and one semicircle for air flow inlet manifold) over the anode surface. To further achieve the detail distributions, the no-dimensional fuel mass flow rates fed to each rib channel ($\dot{m}'_{c\text{-}i} = \dot{m}_{c\text{-}i} / (\dot{m}_{total} / N_l / N_c)$) are shown in Fig. 5b. $\dot{m}_{c\text{-}i}$ is the fuel mass flow rate fed to rib channel *i*. N_l=10 is the total cell layers of the stack. N_c=28 is the number of the rib channels within each piled SOFC unit. The fuel flow distribution results in Fig. 4b shows that: i) for cross section 'f-s-1', most of the fuel flows are concentrated around the feed header and semicircle contact zones. Only very few fuel rates are fed to the zones (i.e., 1-th to 5-th and 23-th t0 28-th rib channels); ii) for cross section 'f-

s-2', too much fuel flows (i.e., around 14% of the total fuel flow fed to each SOFC unit) pass through the semicircle zone, which is labeled as 6-th rib channel. As reported by L. Kang and J. Myung [39, 40], this would lead to greatly reducing the service life of the stack.

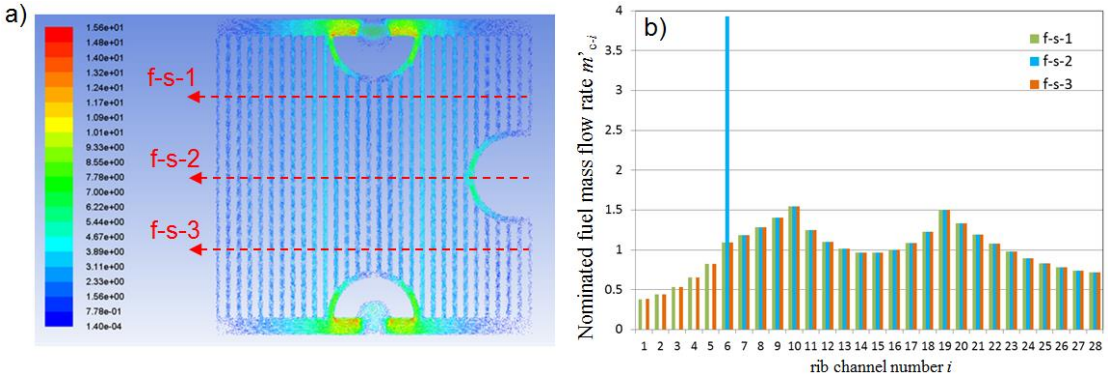

Figure 4. a) the fuel flow velocity distribution over the SOFC unit surface; b) the no-dimensional fuel mass flow rates distribution among the rib channels over three different cross sections.

As the rib channels over each SOFC unit surface are connected in parallel, the standard deviations of the nominated flow rate distributions among the rib channels is adopted to represent the flow distributing quality over each cell unit [32, 34],

$$\sigma_{\dot{m}'_{c-i}} = \left\{ \frac{\sum_{i=1}^{N_c} \left(\dot{m}'_{c-i} - 1 \right)^2}{N_c} \right\}^{1/2}, \qquad (2)$$

The calculated nominated standard deviations for cross sections 'f-s-1', 'f-s-2' and 'f-s-3' are calculated to be 0.2944, 0.6715 and 0.2941, respectively.

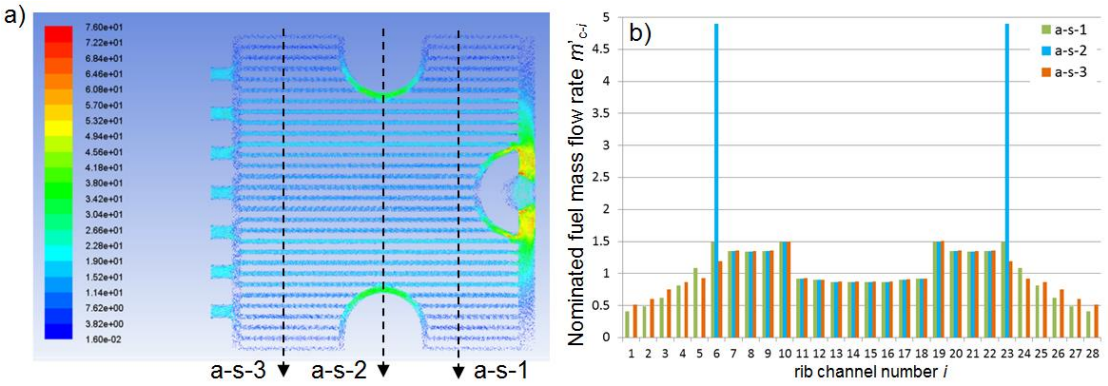

Figure 5. a) the air flow velocity distribution over the SOFC unit surface; b) the no-dimensional air mass flow rates distribution among the rib channels over three different cross sections.

Fig. 5a shows the air flow velocity distribution among the rib channels. Similarly, most of the air flows are concentrated around the two semicircles zones of fuel flow manifolds over the cathode surface. The no-dimensional air mass flow rates fed to each rib channel are shown in Fig. 5b. Obviously, for cross section 'a-s-1', very few fuel rates are fed to the zones far away from the air inlet

manifold. For cross section ‘f-s-2’, however, over 35% air flows of the total air flow fed to each SOFC unit will pass through the two semicircle zones around the fuel manifolds. The calculated nominated standard deviations for cross sections ‘a-s-1’, ‘a-s-2’ and ‘a-s-3’ are calculated to be 0.3493, 1.3286 and 0.2928, respectively.

These results demonstrated that while the fuel and air flow manifolds are penetrated through the SOFC unit plane, the conventional flow path structures in Fig. 3 are impractical because of bad fuel and air distributing designs. It is generally agreed that the flow distribution quality within the SOFC stack can be greatly improved by adding distributors, enlarging the outlet manifold areas, increasing the feed/exhaust header widths, and so on [34, 41]. The flow distribution characteristics within these two different flow path configuration designs will be analyzed by further 3D calculated fluid dynamics calculations, while the fuel and air flow manifolds penetrated through the SOFC unit plane are adopted.

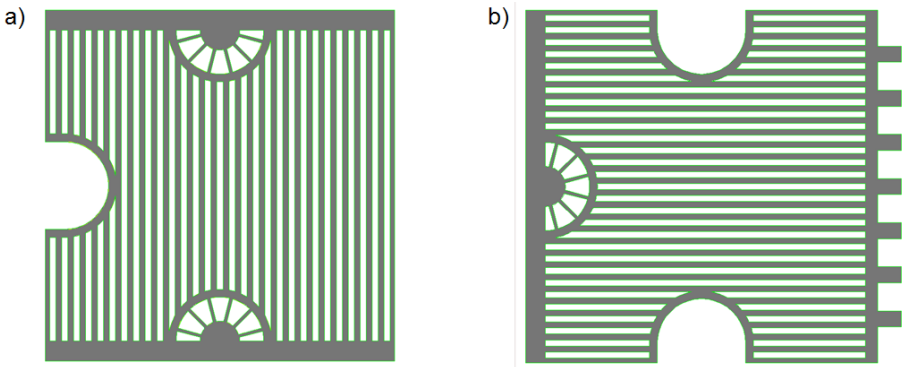

Figure 6. Sketch diagram of a planar SOFC stack design with additional distributors, while the flow manifolds are placed within the cell unit plane: a) configuration of fuel flow distribution path; b) configuration of air flow distribution path.

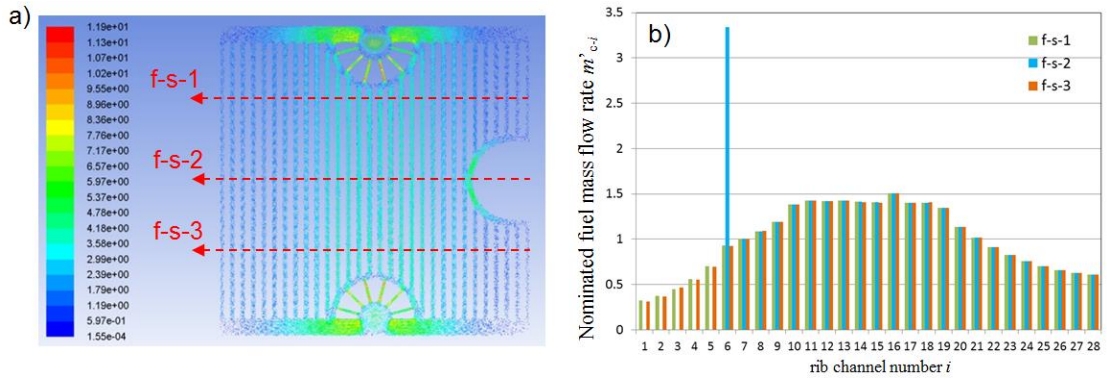

Figure 7. a) the fuel flow velocity distribution over the SOFC unit surface; b) the no-dimensional fuel mass flow rates distribution among the rib channels over three different cross sections.

Fig. 6 illustrates the fuel and air flow path configurations with additional divergent distributors, while the flow manifold penetrates through the SOFC unit plane. The corresponding fuel flow velocity distribution among the rib channels and the normalized fuel mass flow rates $\dot{m}'_{c\text{-}i}$ fed to rib channel i are shown in Fig. 7a and b, respectively. As can be shown in Fig. 7b: i) for cross section ‘f-s-1’, most of the fuel flows are concentrated around the inlet and outlet manifolds zones (i.e., from 7-th to 21-th

rib channels). Only very few fuel rates are fed to the zones (i.e., 1-th to 6-th and 22-th t0 28-th rib channels); ii) for cross section 'f-s-2', too much fuel flows (i.e., around 14% of the total fuel flow fed to each SOFC unit) pass through the semicircle zone, which is labeled as 6-th rib channel. The calculated nominated standard deviations for cross sections 'f-s-1', 'f-s-2' and 'f-s-3' are calculated to be 0.3693, 0.5295 and 0.3700, respectively.

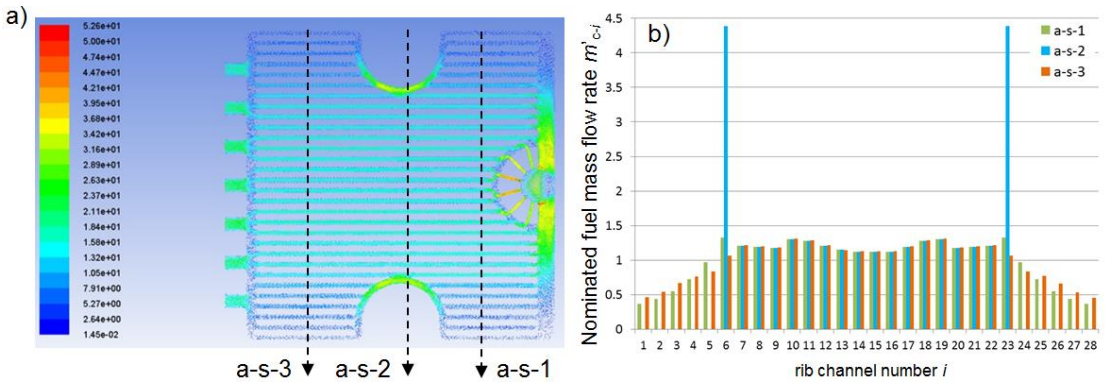

Figure 8. a) the air flow velocity distribution over the SOFC unit surface; b) the no-dimensional air mass flow rates distribution among the rib channels over three different cross sections.

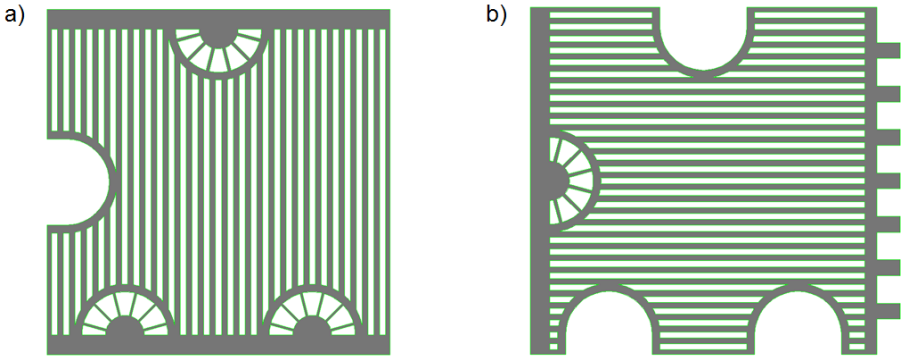

Figure 9. Sketch diagram of a planar SOFC stack design with enlarged overall fuel outlet manifold areas, while places the flow manifolds within the cell unit plane: a) configuration of the fuel flow distribution path; b) configuration of the air flow distribution path.

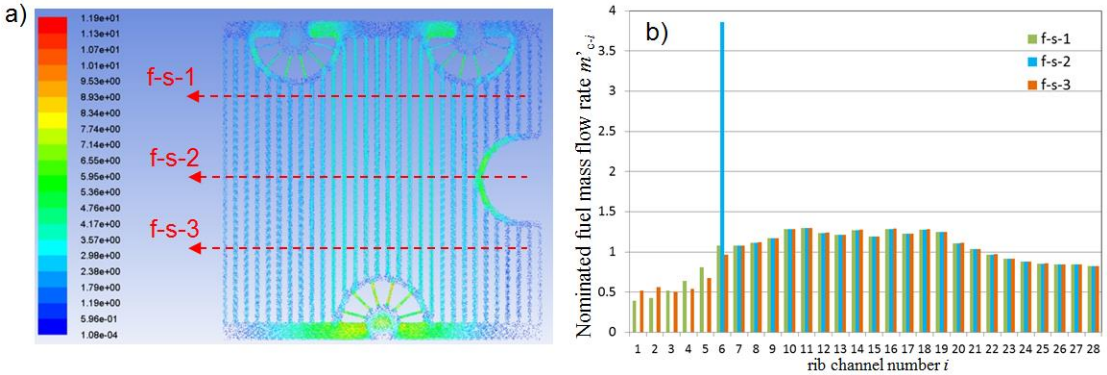

Figure 10. a) the fuel flow velocity distribution over the SOFC unit surface; b) the no-dimensional fuel mass flow rates distribution among the rib channels over three different cross sections.

Fig. 8a and b shows the corresponding calculated air flow velocity distribution over the cathode surface and the normalized air mass flow rates fed to the rib channel $\dot{m}'_{c\text{-}i}$. The nominated standard deviations for cross sections 'a-s-1', 'a-s-2' and 'a-s-3' are calculated to be 0.3219, 1.1459 and 0.2777, respectively.

It is interesting to note that although adopting additional distributors will lead to very different fuel and air flow distribution configurations over the piled SOFC unit surface, over flow rates can also be found around the semicircle zone of the manifolds (shown in Fig. 7a and 8a). This illustrates that unlike many other published reports [41-43], while flow path with the manifold penetrates through the SOFC unit plane, additional divergent distributors may not increase the air and fuel flow feeding quality on the single cell level.

Fig. 9 illustrates the sketch diagrams of both the fuel and air flow manifolds with enlarged overall fuel flow outlet manifold areas, while the flow manifold penetrates through the SOFC unit plane. In this structure, two fuel outlet manifolds are adopted. The corresponding fuel flow velocity distribution among the rib channels and the normalized fuel mass flow rates $\dot{m}'_{c\text{-}i}$ fed to the rib channel are shown in Fig. 10a and b, respectively. Although the fuel flow distribution quality through cross sections ''f-s-1' and 'f-s-3' are slightly improved, there still have over fuel flow rate passed through the semicircle zone in cross sections 'f-s-2'.

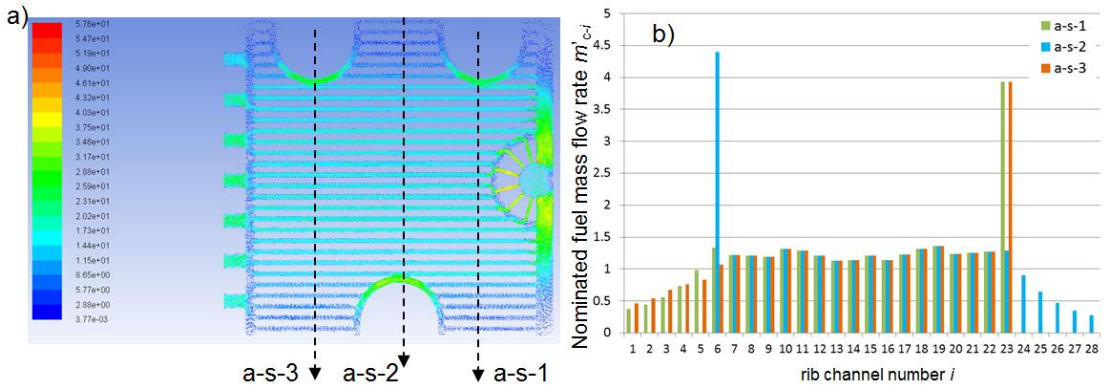

Figure 11. a) the air flow velocity distribution over the SOFC unit surface; b) the no-dimensional air mass flow rates distribution among the rib channels over three different cross sections.

Similarly, Fig. 11a and b shows the corresponding calculated air flow velocity distribution over the cathode surface and the normalized air mass flow rate $\dot{m}'_{c\text{-}i}$ distribution among the rib channel. Obviously, over air flow rates are passed through the .three semicircles of the fuel manifold zones, which would lead them to suffer from serious local failure risks.

4. CONCLUSIONS

The 3D CFD analyzing models for fuel and air flow paths within those SOFC stack designs, which have flow manifolds penetrated through the cell unit plane, had been well developed to analyze their fuel and air distribution qualities. It was concluded that: i) whether the manifolds were penetrated

through the SOFC unit plane would not affect both the fuel and air flow distribution qualities among the piled cell units on stack level. For a small scale planar SOFC stack, the flow distribution quality on stack level was high. The flow distribution quality over each SOFC unit surface, however, should be greatly improved; ii) while the fuel manifolds were placed within the SOFC unit area and penetrated through it, over 31% air would pass through the semicircle zones of the fuel manifold zones; iii) while the air flow manifold was placed within the SOFC unit area, over 14% of the fuel would pass through the semicircle zone of the air manifold zone; iv) while the flow manifolds were penetrated through the cell unit plane, both the fuel and air flow distribution qualities on single cell level would not be greatly improved by adding additional distributors or enlarging the overall outlet manifold areas.

ACKNOWLEDGEMENTS
We gratefully acknowledge the financial support of the Natural Science Foundation of Jiangsu Province General Program (BK20151325), the Jiangsu Province Qinglan Project.

References

1. M. Peksen, *Int. J. Hydrogen Energy* 39 (2014) 5137-5147.
2. D. Chen, Q. Zhang, L. Lu, V. Periasamy, M.O. Tade, Z. Shao, *J. Power Sources* 303 (2016) 305-316.
3. H. Chen, F. Wang, W. Wang, D. Chen, S.-D. Li, Z. Shao, *Appl Energ* 179 (2016) 765-777.
4. W. Kong, W. Zhang, S. Zhang, Q. Zhang, S. Su, *Int. J. Hydrogen Energy* 41 (2016) 16173-16180.
5. D. Chen, Z. Lin, H. Zhu, R.J. Kee, *J. Power Sources* 191 (2009) 240-252.
6. B.B. Xiao, X.B. Jiang, Q. Jiang, *Phys Chem Chem Phys* 18 (2016) 14234-14243.
7. B. Zhu, M.D. Mat, *Int. J. Electrochem. Sci.* 1 (2006) 383-402.
8. L.Q. Fan, Y.P. Xiong, L.B. Liu, Y.W. Wang, M.E. Brito, *Int. J. Electrochem. Sci*. 8 (2013) 8603-8613.
9. T.C. Patil, S.M. Mahajani, S.P. Duttagupta, *Int. J. Electrochem. Sci*. 9 (2014) 8458-8464.
10. W.S. Xia, Y.Z. Yang, Q.S. Wang, *J. Power Sources* 194 (2009) 886-898.
11. D. Chen, H. Wang, S. Zhang, M.O. Tade, Z. Shao, H. Chen, Aiche J. 61 (2015) 3786-3803.
12. D. Chen, H. He, D. Zhang, H. Wang, M. Ni, *Energies* 6 (2013) 1632-1656.
13. S. Su, X. Gao, Q. Zhang, W. Kong, D. Chen, *Int. J. Electrochem. Sci*. 10 (2015) 2487-2503.
14. X.L. Sun, S. Li, J.C. Sun, X.R. Liu, B. Zhu, *Int. J. Electrochem. Sci*. 2 (2007) 462-468.
15. L. Blum, H.P. Buchkremer, S. Gross, A. Gubner, L.G.J. de Haart, H. Nabielek, W.J. Quadakkers, U. Reisgen, M.J. Smith, R. Steinberger-Wilckens, R.W. Steinbrech, F. Tietz, I.C. Vinke, *Fuel Cells* 7 (2007) 204-210.
16. Xiang Gao, Qiang Zhang, Wenxuan Zhang, D. Chen, *Int. J. Electrochem. Sci*. 10 (2015) 7521-7534.
17. K. Liu, Z. Wang, W. Tang, Y. Zhang, G. Wang, *Ocean Engineering* 99 (2015) 44-54.
18. S. Shichuan, W. Liang, N. Yuhong, G. Xiang, *Safety Science* 50 (2012) 12-18.
19. J. Park, J. Bae, *Int. J. Hydrogen Energy* 37 (2012) 1717-1730.
20. H. Hirata, T. Nakagaki, M. Hori, J. Power Sources 102 (2001) 118-123.
21. H. Hirata, T. Nakagaki, M. Hori, J. Power Sources 83 (1999) 41-49.
22. K.P. Recknagle, R.E. Williford, L.A. Chick, D.R. Rector, M.A. Khaleel, J. Power Sources 113 (2003) 109-114.
23. L. Blum, W.A. Meulenberg, H. Nabielek, R. Steinberger‐Wilckens, Int. J. App. Cer. Tech. 2 (2005) 482-492.
24. C.-K. Lin, T.-T. Chen, Y.-P. Chyou, L.-K. Chiang, *J. Power Sources*, 164 (2007) 238-251.

25. P. Batfalsky, J. Malzbender, N.H. Menzler, *Int. J. Hydrogen Energy*, 41 (2016) 11399-11411.
26. Z. Wang, K. Liu, C. Ji, D. Chen, G. Wang, C.G. Soares, *Ocean Engineering*, 127 (2016) 212-225.
27. F.X. Miao, *Int. J. Electrochem. Sci.*, 8 (2013) 11814-11822.
28. W. Wu, W. Guan, W. Wang, *J. Power Sources*, 279 (2015) 540-548.
29. D. Chen, L. Lu, J. Li, Z. Yu, W. Kong, H. Zhu, *J. Power Sources*, 196 (2011) 3178–3185.
30. D. Yan, Z. Bin, D. Fang, J. Luo, X. Wang, J. Pu, B. Chi, L. Jian, Y. Zhang, *Int. J. Hydrogen Energy*, 38 (2013) 660-666.
31. L. Jin, W. Guan, J. Niu, X. Ma, W.G. Wang, *J. Power Sources*, 240 (2013) 796-805.
32. Z. Yu, *Int. J. Electrochem. Sci.*, (2016) 9100-9109.
33. D. Chen, Q. Zeng, S. Su, W. Bi, Z. Ren, *Appl. Energ.*, 112 (2013) 1100-1107.
34. S. Su, H. He, D. Chen, W. Zhu, Y. Wu, W. Kong, B. Wang, L. Lu, *Int. J. Hydrogen Energy*, 40 (2015) 577-592.
35. L. Kang, W. Fenghui, Z. Xiang, L. Yongjun, *Int. J. Electrochem. Sci.*, 11 (2016) 1382 - 1394.
36. W. Kong, Q. Zhang, X. Gao, J.Y. Zhang, D.F. Chen, S.C. Su, *Int. J. Electrochem. Sci.*, 10 (2015) 5800-5811.
37. S.Q. Yang, T. Chen, Y. Wang, Z.B. Peng, W.G. Wang, Int. *J. Electrochem. Sci.*, 8 (2013) 2330-2344.
38. G.B. Jung, L.H. Fang, C.Y. Lin, X.V. Nguyen, C.C. Yeh, C.Y. Lee, J.W. Yu, S.H. Chan, W.T. Lee, S.W. Chang, I.C. Kao, *Int. J. Electrochem. Sci.*, 10 (2015) 9089-9104.
39. J.H. Myung, H.J. Ko, J.J. Lee, S.H. Hyun, *Int. J. Electrochem. Sci.*, 6 (2011) 1617-1629.
40. L. Kang, *Int. J. Electrochem. Sci.*, 10 (2016) 5596-5606.
41. C.M. Huang, S.S. Shy, H.H. Li, C.H. Lee, *J. Power Sources*, 195 (2010) 6280-6286.
42. C.M. Huang, S.S. Shy, C.H. Leeb, *J. Power Sources*, 183 (2008) 205-213.
43. M. Dudek, P. Tomczyk, K.L. Juda, R. Tomov, B.A. Glowacki, S. Batty, P. Risby, R. Socha, *Int. J. Electrochem. Sci.*, 7 (2012) 6704-6721.